NeuroImage 52 (2010) 562–570

Contents lists available at ScienceDirect

NeuroImage

journal homepage: www.elsevier.com/locate/ynimg

Imaging brain hemodynamic changes during rat forepaw electrical stimulation using functional photoacoustic microscopy

Lun-De Liao [a,b,1], Meng-Lin Li [c,1], Hsin-Yi Lai [a], Yen-Yu I. Shih [d], Yu-Chun Lo [e], Siny Tsang [f], Paul Chang-Po Chao [a], Chin-Teng Lin [a,b], Fu-Shan Jaw [e], You-Yin Chen [a,*]

[a] Department of Electrical Engineering, National Chiao Tung University, No. 1001, Ta-Hsueh Rd., Hsinchu 300, Taiwan ROC
[b] Brain Research Center, National Chiao Tung University, No. 1001, Ta-Hsueh Rd., Hsinchu 300, Taiwan ROC
[c] Department of Electrical Engineering, National Tsing Hua University, No. 101, Sec. 2, Kuang-Fu Rd., Hsinchu 300, Taiwan ROC
[d] Research Imaging Institute, University of Texas Health Science Center at San Antonio, 8403 Floyd Curl Drive, San Antonio, Texas 78229-3900, USA
[e] Institute of Biomedical Engineering, College of Medicine, National Taiwan University, No.1, Sec. 1, Jen-Ai Rd., Taipei 100, Taiwan ROC
[f] College of Criminal Justice, Sam Houston State University, Huntsville, Texas 77341-2296, USA

ARTICLE INFO

Article history:
Received 28 December 2009
Revised 7 March 2010
Accepted 20 March 2010
Available online 31 March 2010

Keywords:
Functional photoacoustic microscopy (fPAM)
Electrical stimulation
Total hemoglobin concentration (HbT)
Hemoglobin oxygen saturation (SO_2)

ABSTRACT

The present study reported the development of a novel functional photoacoustic microscopy (fPAM) system for investigating hemodynamic changes in rat cortical vessels associated with electrical forepaw stimulation. Imaging of blood optical absorption by fPAM at multiple appropriately-selected and distinct wavelengths can be used to probe changes in total hemoglobin concentration (HbT, i.e., cerebral blood volume [CBV]) and hemoglobin oxygen saturation (SO_2). Changes in CBV were measured by images acquired at a wavelength of 570 nm (λ_{570}), an isosbestic point of the molar extinction spectra of oxy- and deoxy-hemoglobin, whereas SO_2 changes were sensed by pixel-wise normalization of images acquired at λ_{560} or λ_{600} to those at λ_{570}. We demonstrated the capacity of the fPAM system to image and quantify significant contralateral changes in both SO_2 and CBV driven by electrical forepaw stimulation. The fPAM system complements existing imaging techniques, with the potential to serve as a favorable tool for explicitly studying brain hemodynamics in animal models.

Introduction

Imaging of hemoglobin oxygen saturation (SO_2) changes is crucial to understanding brain function. It has a broad range of medical applications, such as monitoring therapeutic interventions of major diseases (Ermilov et al., 2009; Foo et al., 2004; Li et al., 2007; Menon and Fraker, 2005; Tandara and Mustoe, 2004). Using imaging techniques to directly measure SO_2 changes also facilitate disease diagnosis (Cina et al., 1984; Lee et al., 2009; Tandara and Mustoe, 2004). Functional magnetic resonance imaging (fMRI) (Hyder et al., 1994; Nair and Duong, 2004) and diffusion optical imaging (DOI) (Culver et al., 2005; Siegel et al., 2003) can be used to assess changes of oxygenation *in vivo*. These techniques are increasingly used to study effects in preclinical stages during the rapid development of novel drugs and therapeutic interventions in animal models. Hyder et al. first demonstrated that blood oxygenation level-dependent (BOLD) fMRI was a reliable tool for studying cortical activation in a rat model driven by forepaw electrical stimulation (Hyder et al., 1994). The relative cerebral blood volume (CBV) changes due to forepaw stimulation have also been studied with the aid of exogenous contrast agents (Keilholz et al., 2006; Mandeville et al., 2005). Although fMRI can measure BOLD and CBV separately, it is still difficult to isolate pure SO_2 changes (Haacke et al., 1998; Keilholz et al., 2006; Langham et al., 2009; Mandeville et al., 2005). The DOI technique can directly acquire SO_2 signals, but due to strong optical scattering, its spatial resolution is insufficient to delineate the fine details of specific brain structures (Gratton and Fabiani, 1998; Wang and Wu, 2007). Therefore, a better technique for direct SO_2 imaging is needed.

Photoacoustic imaging is an optical absorption-based hybrid imaging technique that combines the advantages of optics and ultrasound—namely, high optical absorption contrast and ultrasonic spatial resolution up to a penetration depth of ~5 cm (Wang, 2009a,b; Zhang et al., 2006). A pulsed laser in the visible or near-infrared (NIR) range is used to irradiate a biological sample, and optical absorption in biological tissue induces photoacoustic (PA) waves via a thermo-elastic effect (Wang, 2009b). From PA signals detected by highly-sensitive ultrasound receivers, the distributions of optical absorptions in the sample can be reconstructed (Wang, 2008). Photoacoustic imaging is marked by a high optical absorption contrast of biological tissue, instead of the low acoustical contrast of ultrasound imaging; whereas the spatial resolution of photoacoustic imaging is

* Corresponding author. Fax: +886 3 612 5059.
E-mail address: irradiance@so-net.net.tw (Y.-Y. Chen).
[1] Contributed equally to this work.

1053-8119/$ – see front matter © 2010 Elsevier Inc. All rights reserved.
doi:10.1016/j.neuroimage.2010.03.065

determined primarily by the ultrasonic characteristics of generated PA waves rather than the optical diffusion typical of the optical imaging (Wang 2008, 2009a). By taking advantage of the ultrasonic detection, PA imaging can provide better spatial resolution than DOI. In addition, by leveraging the intrinsic oxygen-dependent spectral absorption properties of hemoglobin, it has been shown that this technique can detect changes in SO_2 and total hemoglobin concentration (HbT) related to blood volume and flow independently in single vessels (Fainchtein et al., 2000). This is a fascinating feature for a label-free functional brain imaging system. Recently, Maslov et al. invented a reflection-mode confocal PA-microscopic imaging technique with dark field illumination and a high-frequency (>20 MHz) ultrasound transducer, providing high spatial resolution of a few tens of micrometers at a penetration depth of a few millimeters (Maslov et al., 2005). Stein et al. have demonstrated the capability of such a microscopic technique to track blood oxygenation dynamics in a mouse brain undergoing global hypoxic and hyperoxic challenges, showing its potential for probing brain hemodynamic changes for specific brain activation (Stein et al., 2008, 2009).

In this study, we established a functional photoacoustic microscopy (fPAM) system that was able to assess functional changes in SO_2 and CBV corresponding to specific brain activation. Electrical forepaw stimulation was employed to activate the contralateral primary somatosensory cortex. We also discussed details of the functional imaging analysis method for SO_2 and CBV changes. The aim of the present study was to determine whether the fPAM system could be used to separately visualize changes in SO_2 and CBV resulting from neuronal activation. Our results showed that fPAM can robustly probe changes in SO_2 and CBV in vascular segments of cortical areas by using intrinsic optical absorption contrast. This technique has potential to further our understanding of brain–neurovascular coupling, as well as to monitor disease progression in small animal models.

Materials and methods

Dark field confocal functional photoacoustic microscopy system

The current 25 MHz dark field confocal fPAM system for imaging functional changes in cortical vessels, as shown in Fig. (1), consisted of a laser pulse generation and delivery, a PA signal reception, and an image reconstruction and display. The system is capable of providing A-scan, B-scan (i.e., two-dimensional images where one axis is lateral to the scanning distance and the other is the imaging depth), and C-scan (i.e., three-dimensional images) images of the area of inspection. The whole system was controlled by custom-developed software based on MATLAB® (R2007a, The MathWorks, USA). An optical parametric oscillator (Surlite OPO Plus, Continuum, USA) pumped by a frequency-tripled Nd:YAG Q-switched laser (Surlite II-10, Continuum, USA) was utilized to provide laser pulses at laser wavelengths of 560, 570, and 600 nm (λ_{560}, λ_{570} and λ_{600}), with a pulse width of ~4 ns and a pulse repetition rate of 10 Hz. At the selected wavelengths, blood is dominantly and strongly absorbant, thus guaranteeing that detected PA signals mainly come from blood vessels. The detected PA signals at λ_{560} and λ_{600} were sensitive to changes in SO_2, whereas those at λ_{570} were dominated by changes in CBV (for details please refer to the Appendix). Laser energy was delivered by a 1 mm multimode fiber. The fiber tip was coaxially positioned with a convex lens, an axicon, a plexiglass mirror, and a 25 MHz focused ultrasonic transducer (v324, Olympus, USA) on an optical bench, which created dark field illumination and made the

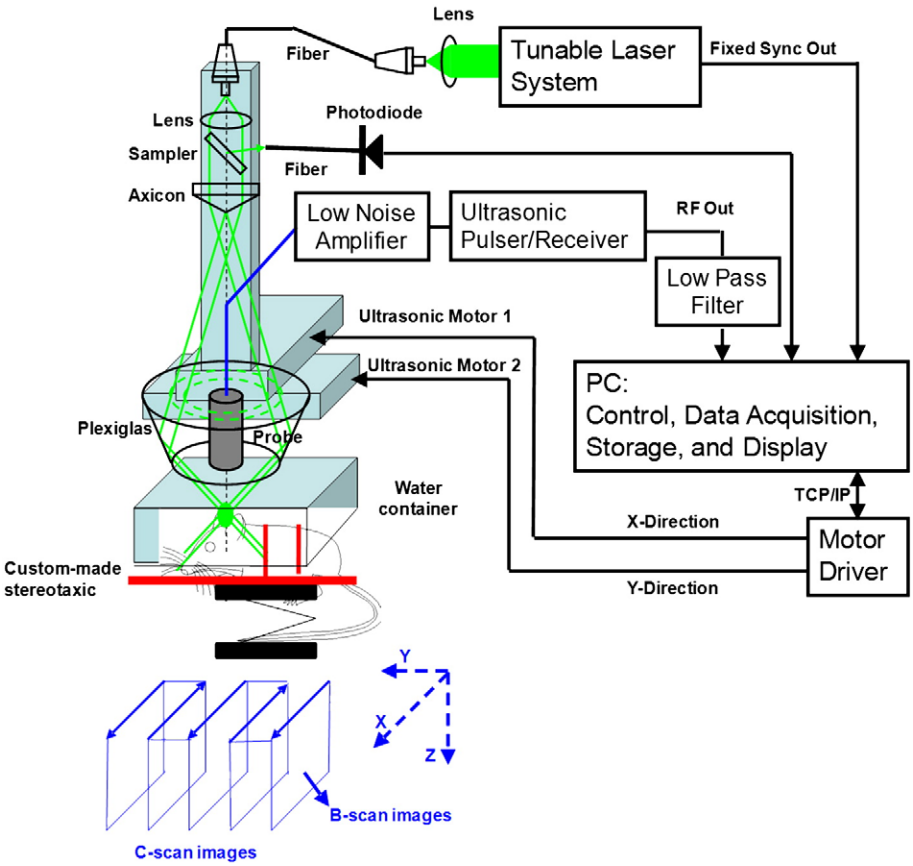

Fig. 1. Experimental setup of the fPAM. A window at the bottom of the water container was sealed with an optically and ultrasonically transparent, disposable polyethylene film. After commercially-available ultrasound gel was applied to the brain for acoustic coupling, the brain was placed between the water container and custom-made stereotaxic apparatus for imaging. The laser was pulsed with a pulse repetition rate of 10 Hz and coupled by a lens to an optical fiber to illuminate the rat's brain. PA waves were detected by a 25 MHz transducer and then through the A/D card to the PC for further data analysis.

light confocal with the ultrasonic transducer. The optical bench was fixed on a three-dimensional precision translation stage, upon which the *x*- and *y*-axes were motorized and the *z*-axis could be manually adjusted with a micrometer. The 25 MHz ultrasonic transducer had a −6dB fractional bandwidth of 55%, a focal length of 12.7 mm and a 6 mm active element, offering an axial resolution of 68 μm and a lateral resolution of 171 μm for fPAM. This fPAM had a 6 mm penetration depth, and the achievable signal-to-noise ratio (SNR) at the depth of 5.88 mm is about 13.39 dB where the SNR was defined as the ratio of the signal peak value to the root-mean-square value of the noise (Wang, 2009c). A photodiode (DET36A/M, Thorlabs, USA) was used to monitor fluctuations of the laser energy. The incident energy density on the sample surface was less than 6 mJ/cm^2, which was well within the ANSI safety limit of 20 mJ/cm^2. During imaging, the transducer was immersed in an acrylic water tank, with a hole at the bottom sealed with a piece of 15 μm thick polyethylene film. The hole served as an acoustic window. The rat's skull was removed, coated with a thin layer of ultrasonic gel, and attached to the thin film to ensure good coupling of PA waves. The PA signals received by the ultrasonic transducer were pre-amplified by a low-noise amplifier (noise figure 1.2 dB, gain 55 dB, AU-3A-0110, Miteq, USA), cascaded to an ultrasonic pulser/receiver (5073 PR, Olympus, USA), low-pass filtered, digitized by a PC-based 14 bit analog to digital (A/D) card (CompuScope 14200, GaGe, USA), sampled at 200 MHz, and then stored in the PC. Before any further signal processing, PA signal variations caused by laser energy instability were compensated for with the recorded photodiode signals. The PA images shown in the following sections were taken without signal averaging, and the amplitudes of the envelope-detected PA signals were used in the subsequent functional imaging analysis.

Experimental animals

Six male Wistar rats (National Laboratory Animal Center, Taiwan), weighing 250–350 g, were used. The animals were housed at a constant temperature and humidity with free access to food and water. Before imaging experiments, the rats fasted for 24 h but were given water ad libitum. All animal experiments were conducted in accordance with guidelines from Animal Research Committee of National Chiao Tung University and National Tsing Hua University.

The animals were initially anesthetized by 3% isoflurane. A PE-50 catheter was inserted in the left femoral vein for subsequent α-chloralose anesthesia (70 mg/kg). Anesthetized rats were mounted on the custom-made acrylic stereotaxic head holder, and the skin and muscle were cut away from the skull to expose the bregma landmark. The anteroposterior (AP) distance between the bregma and the interaural line (Paxinos and Watson, 2007) was directly surveyed. The bregma was 9.3 ± 0.12 mm (mean ± standard deviation [SD]) anterior to the interaural line (data not published). Furthermore, a craniotomy was performed for each animal, and a bilateral cranial window of approximately 10 (horizontal) × 8 (vertical) mm size was made with a high-speed drill. Fig. 2(A) depicted how animals' heads were positioned in the fPAM system, which was shown in Fig. 2(B). After the rat was secured to the stereotaxic frame and placed on the bed pallet, the pallet was moved until the crosshair of the laser alignment system was positioned at the bregma, which was 9 mm anterior to an imaginary line drawn between the centers of each ear bar (the interaural line). The interaural and bregma references were then used to position the heads in the fPAM system, without additional surgery, in the following experiments.

Functional PA imaging and statistical analysis

After bregma positioning, the PA C-scan (i.e., two-dimensional scanning) was performed to acquire functional and reference images. It was also used to ensure that the rat's head was located at the focal zone of the 25-MHz transducer. Fig. 3(A) showed an open-skull anatomical photograph of a prepared rat brain, taken prior to the imaging procedure. An *in vivo* maximum-amplitude projected C-scan image of the cortex, acquired at λ_{570}, was shown in Fig. 3(B) and depicted the 8.5 × 5.5 mm ranges. The PA-projected C-scan image included 85 B-scan images with scans separated by 100 μm. As shown in Fig. 3(B), cortical blood vessels as indicated by the solid arrows in Fig. 3(A) were imaged. In addition, some branches of these vessels could be seen in the projected C-scan image.

Next, a pair of needle electrodes was inserted under the skin of the rat's left forepaw; electrical stimulation was applied using a stimulator (Model 2100, A-M Systems, USA) with a monophasic constant current at 5 mA pulses with a width of 0.2 ms at a frequency of 3 Hz. For acquiring fPAM image, a block design paradigm was proposed and evaluated with forepaw electrical stimulation. Each stimulation protocol consisted of six blocks, alternating between the 24 s baseline (stimulation-OFF) and electrical stimulation task (stimulation-ON) blocks. In the current fPAM system, data acquisition took 14 s for a PA B-scan image with 135 scan lines (8 mm width). PAM images were acquired in each block to assess for stimulation-induced changes in the physiological fluctuation signal from vascular segments in specific cortical areas. The block design paradigm and the PA imaging protocol were shown in Fig. 4. For a given brain section, the same functional imaging procedure was repeated three times.

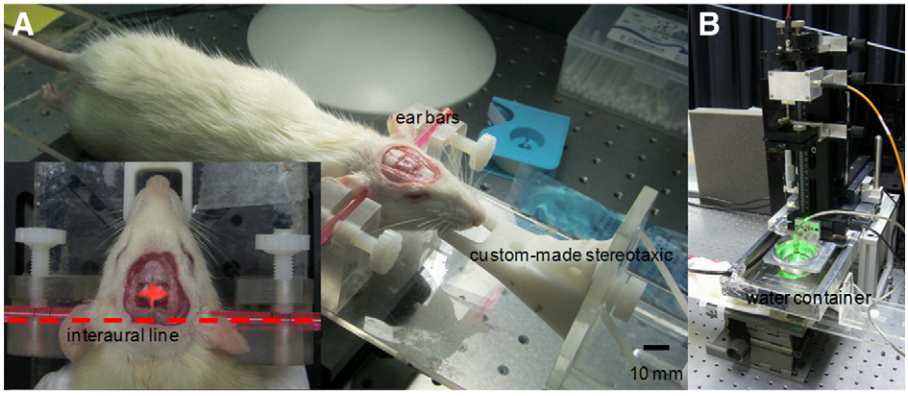

Fig. 2. Illustration of precise animal positioning (A) and photo of the scanning head of the fPAM system (B). (A) The rat head was fixed firmly to the custom-made stereotaxic apparatus with two ear bars in an identified interaural line through the external auditory meatus. The PA B-scan image through the bregma site served as a reference position for other B-scan images. (B) A window at the bottom of the water container was sealed with an optically and ultrasonically transparent, disposable polyethylene film. After commercially-available ultrasound gel was applied to the rat's brain for acoustic coupling, the rat's head was placed between the water container and the bed pallet of the custom-made stereotaxic apparatus. The bregma 9 mm anterior to the interaural line was positioned by the independent laser alignment system. The interaural and bregma references were then used to position the head in the fPAM system to ensure the positions of acquired functional images.

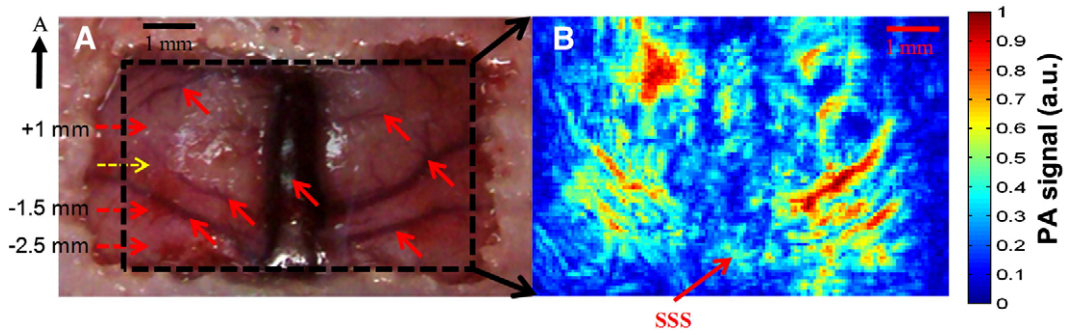

Fig. 3. Comparison of the open-skull photograph with PA-projected C-scan image acquired at λ_{570}. The left black arrow pointed in the rostral direction. (A) An open-skull photograph of the brain surface. The yellow dashed line indicated the position of the bregma. Functional B-scan images were acquired by scanning along the red dashed lines, which were +1, −1.5, and −2.5 mm from the bregma, respectively. The red solid arrows indicated the cortical vessels. (B) *In vivo* PA-projected C-scan image of the blood vessels in the superficial layer of the cortex, acquired at λ_{570}. The vascular patent has been imaged. Compared to the red solid arrows in (A), some branches of the vessels were also imaged more clearly.

Reference images ($I_{R(570)}$) at λ_{570} for a stimulation-OFF ($I_{R(570),\ \text{stimulation-OFF}}$) and a stimulation-ON ($I_{R(570),\ \text{stimulation-ON}}$) block were acquired. For the same region, respective images (I) at λ_{560} or λ_{600} for stimulation-OFF ($I_{(560\text{ or }600),\ \text{stimulation-OFF}}$) and stimulation-ON ($I_{(560\text{ or }600),\ \text{stimulation-ON}}$) blocks were also acquired. Functional images ($\Delta I_{F(560\text{ or }600)}$) were then constructed according to the following equation:

$$\Delta I_{F(560\text{ or }600)} = \frac{I_{(560\text{ or }600\,\text{nm})\ \text{stimulation-ON}}}{I_{R(570\,\text{nm})\ \text{stimulation-ON}}} - \frac{I_{(560\text{ or }600\,\text{nm})\ \text{stimulation-OFF}}}{I_{R(570\,\text{nm})\ \text{stimulation-OFF}}} = I_{F(560)\ \text{stimulation-ON}} - I_{F(560)\ \text{stimulation-OFF}}. \quad (1)$$

To identify PA signal changes in response to left forepaw stimulation, functional images at three different positions, bregma + 1 mm, bregma − 1.5 mm, and bregma − 2.5 mm were acquired (as indicated in Fig. 3(A)). To accurately identify regions of interest (ROIs) for PA signal changes in coronal brain-image slices, fusions of PA images and a rat brain atlas (Paxinos and Watson, 2007) were performed by a modified laboratory-built ISPMER image processing system (Shih et al., 2007; Shih et al., 2008). Fused images were adopted to define the anatomical borders of the primary somatosensory cortex for the forepaw (S1FL) from images scanned at bregma + 1 mm and bregma − 1.5 mm, as well as the somatosensory cortex of the trunk (S1Tr) area from images acquired at bregma − 2.5 mm.

The experiment was designed to quantitatively compare differences in PA signal ($I_{R(570)}$) changes in ROIs of S1FL and S1Tr resulting from stimulation of the left forepaw. Statistical significance was assessed using paired *t*-test, with significance defined as a probability (p) value of <0.05. Side-to-side differences in PA signals ($I_{R(570)}$) of bilateral cortical areas were also examined using a paired *t*-test ($p<0.05$, $n=6$). The significance of changes observed in response to electrical stimulation in fPAM signals ($\Delta I_{F(560\text{ or }600)}$) of bilateral S1FL and S1Tr were compared with Wilcoxon matched-pairs signed-rank test (two-tailed, $p<0.05$, $n=6$). All statistical analyses were performed using SPSS (version 10.0, SPSS®, USA).

Results

Imaging of the blood vasculature in the cerebral cortex

The open-skull window of the rat cortical surface was shown in Fig. 3(A); many blood vessels on this surface were observable. The superior sagittal sinus (SSS) and other big vessels on the cortical surface could be observed visually, as indicated by red solid arrows in Figs. 3(A) and (B). The vasculature of the cortex in the open window was imaged *in vivo* by fPAM at λ_{570}, as shown in Fig. 3(B). In Fig. 3(B), cortical blood vessels indicated by the solid arrows in Fig. 3(A) were imaged. In addition, some branches of these vessels were also visualized in the projected C-scan image. However, SSS images obtained by the current fPAM were not satisfactory; the imaging results were similar to those obtained in Stein et al. (2009). The geometric focus and the finite detection bandwidth of the ultrasound transducer used may be accounted for the weakness of the detected PA signals from the SSS.

$I_{R(570)}$ PA signal changes in the bilateral brain regions under Stimulation-OFF and Stimulation-ON conditions

The $I_{R(570)}$ images for the three brain sections of interest, for the stimulation-OFF and stimulation-ON conditions, were shown in the upper and lower panels of Fig. 5(A), respectively. Note that $I_{R(570)}$ is

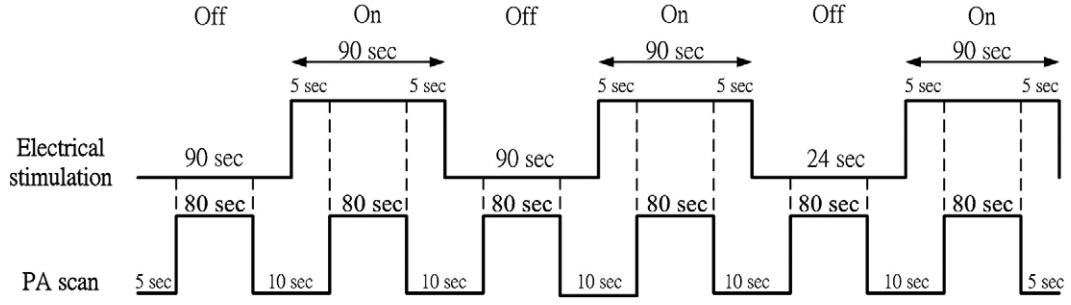

Fig. 4. fPAM data collected with a block design paradigm. The block design utilized an electrical forepaw stimulation task. The task began at the baseline "Stimulation-OFF" state; the active "Stimulation-ON" state was a constant 3 Hz electrical pulse train. PA scan section was performed for 14 s in every block. There was a 5 s lapse between the PA scan and the block design paradigm. Scanning started 5 s after the task began, and the scanning stopped 5 s prior to the end of the task.

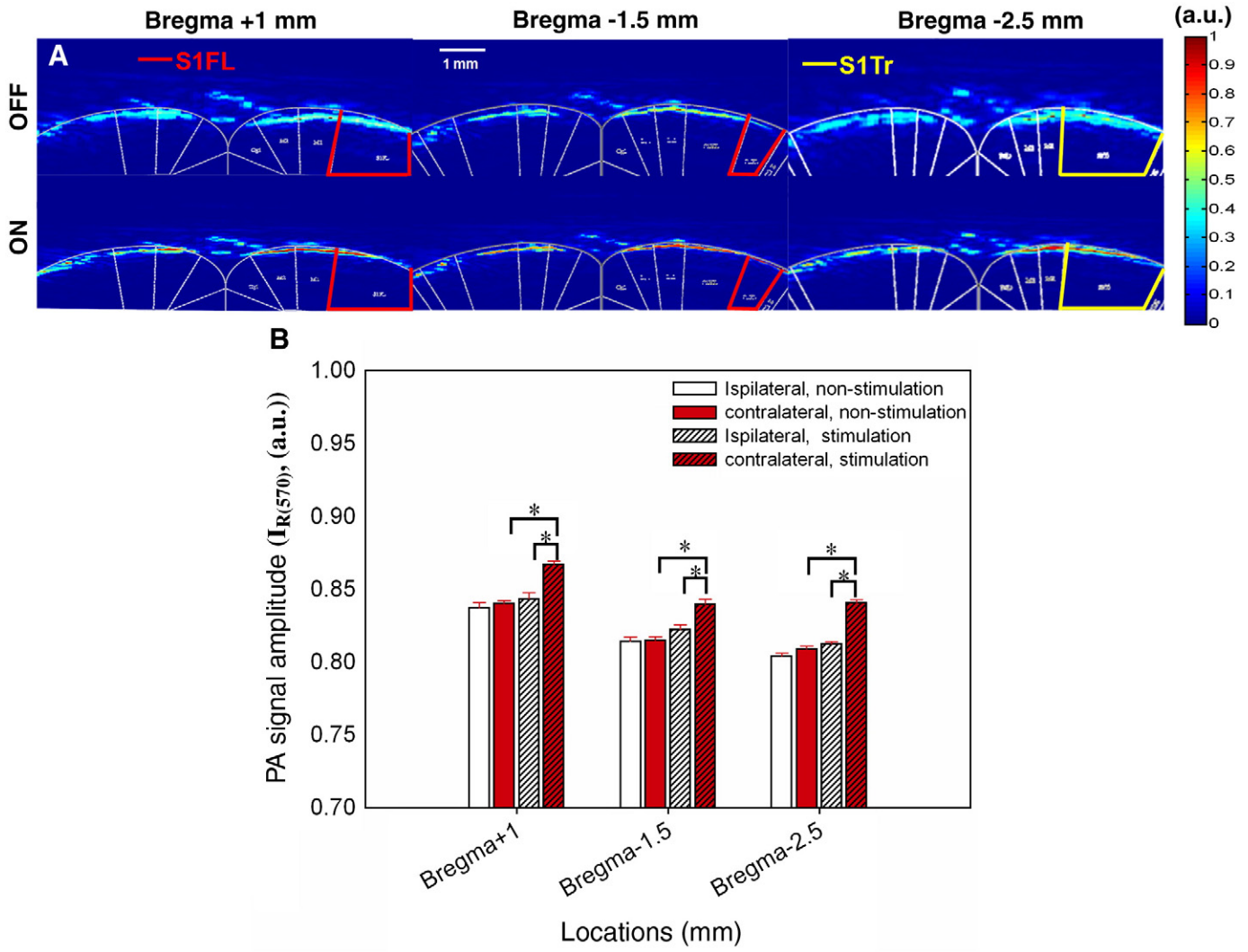

Fig. 5. (A) *In vivo* $I_{R(570)}$ PA B-scan images registered and fused with the rat atlas at the positions of bregma + 1 mm, − 1.5 mm, and − 2.5 mm for stimulation-OFF (upper panels) and stimulation-ON (lower panels). Strong CBV changes in ROIs of S1FL were indicated in red at bregma + 1 mm and − 1.5 mm, and S1Tr were indicated in yellow at bregma − 2.5 mm were found during stimulation (B) Quantitative analysis of the $I_{R(570)}$ PA signal changes in the bilateral ROIs between the stimulation-ON and -OFF conditions. PA signals in the bilateral regions of the primary somatosensory cortex of the forepaw (S1FL) from image sections at bregma + 1 mm and bregma − 1.5 mm and the somatosensory cortex of the trunk (S1Tr) area at bregma − 2.5 mm were used for statistical analyses. Standard deviations were indicated by the error bars; $^*p<0.05$ (paired *t*-test, $n=6$).

proportional to CBV. The contralateral S1FL regions at the imaging positions of bregma + 1 mm and bregma − 1.5 mm and S1Tr at bregma − 2.5 mm showed significant differences in PA signals between the upper and lower panels (i.e., stimulation-OFF and stimulation-ON blocks).

The PA signals in the bilateral regions of the primary somatosensory cortex of the forepaw (S1FL) from image sections at bregma + 1 mm and bregma − 1.5 mm and the somatosensory cortex of the trunk (S1Tr) area at bregma − 2.5 mm were examined. The results were shown in Fig. 5(B). Quantitative analysis showed that between the conditions of stimulation-ON and stimulation-OFF, significant functional changes of $I_{R(570)}$ detected in the contralateral S1FL regions at the imaging positions of bregma + 1 mm and bregma − 1.5 mm and S1Tr at bregma − 2.5 mm were 3.580 ± 0.005%, 3.450 ± 0.008% and 3.510 ± 0.005% (mean ± SD), respectively($p=0.0003$, 0.0001 and 0.0010, respectively, paired *t*-test; $n=6$), as shown in Fig. 5(B). Moreover, no significant bilateral differences in the S1FL regions located at bregma + 1 mm and bregma − 1.5 mm and S1Tr at bregma − 2.5 mm were detected under the stimulation-OFF condition; less bilateral differences of $I_{R(570)}$ were 0.780 ± 0.008%, 0.650 ± 0.006% and 0.890 ± 0.005% ($p=0.074$, 0.085 and 0.860, respectively, paired *t*-test; $n=6$), respectively. In addition, bilateral differences between the S1FL regions at bregma + 1 mm and bregma − 1.5 mm and S1Tr at bregma − 2.5 mm detected under stimulation-ON were approximately 3.120 ± 0.004%, 2.930 ± 0.006% and 3.230 ± 0.005%, all of which were statistically significant ($p=0.0031$, 0.0001 and 0.0005, respectively, paired *t*-test; $n=6$).

$\Delta I_{F(560\ or\ 600)}$ PA signal changes in the bilateral brain region during Stimulation-OFF and Stimulation-ON conditions

The *in vivo* $\Delta I_{F(560)}$ and $\Delta I_{F(600)}$ functional images used for probing the SO_2 changes were shown in the upper and lower panels of Fig. 6(A), respectively. The PA functional signals of $\Delta I_{F(560)}$ and $\Delta I_{F(600)}$ were negative in the contralateral S1FL region at the bregma + 1 mm brain section, as shown in the leftmost panels of Fig. 6(A), whereas the signals were positive in the contralateral S1FL regions at the bregma − 1 mm section and in the contralateral S1Tr region at the bregma − 2.5 mm section, as shown in the middle and rightmost panels of Fig. 6(A). The negative values in $\Delta I_{F(560)}$ and $\Delta I_{F(600)}$ (i.e., a decrease in $I_{F(560)}$ or $I_{F(600)}$) indicated increases in SO_2 levels, and vice versa (please refer to the Appendix for elaboration).

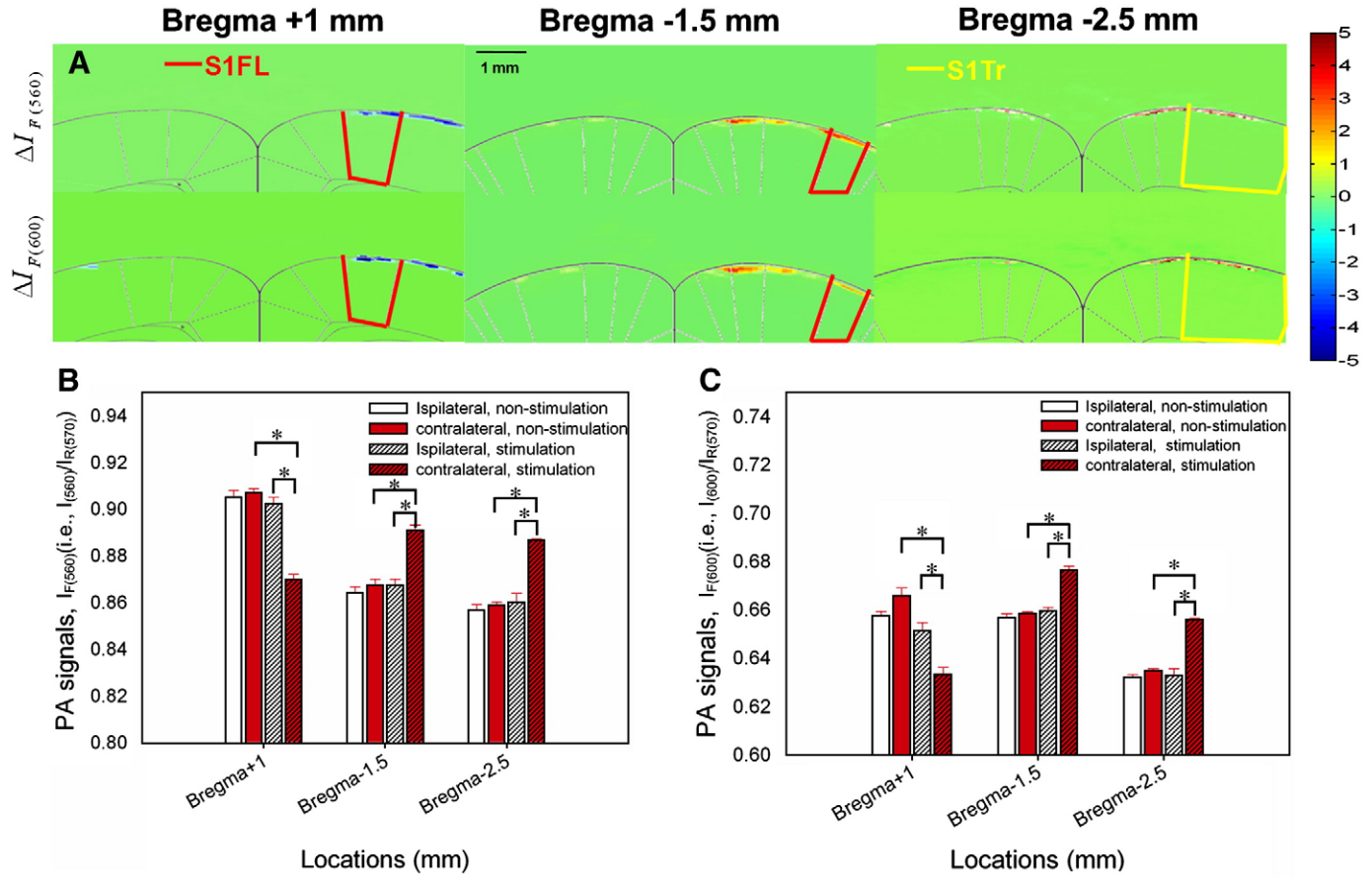

Fig. 6. (A) *In vivo* functional $\Delta I_{F(560)}$ (upper panels) and $\Delta I_{F(600)}$ (lower panels) PA B-scan images registered and fused with the rat atlas at bregma + 1 mm, − 1.5 mm, and − 2.5 mm. SO_2 changes were observed in ROIs of S1FL, as indicated in red at bregma + 1 mm and − 1.5 mm; ROIs of S1Tr was indicated in yellow at bregma-2.5 mm during stimulation. (B) Quantitative analysis of the $I_{F(560)}$ PA signal changes in the bilateral ROIs between the stimulation-ON and -OFF conditions. (C) Quantitative analysis of the $I_{F(600)}$ PA signal changes in the bilateral ROIs between the stimulation-ON and -OFF conditions. $I_{F(560\text{ or }600)}$ PA signals in the bilateral regions of the primary somatosensory cortex of the forepaw (S1FL) from image sections at bregma + 1 mm and bregma − 1.5 mm and the somatosensory cortex of the trunk (S1Tr) area at bregma − 2.5 mm were used for statistical analyses. Standard deviations were indicated by the error bars; $^*p<0.05$ (Wilcoxon matched-pairs signed-rank test, $n=6$).

Quantitative analyses of the $I_{F(560)}$ and $I_{F(560)}$ PA signal changes in the bilateral ROIs between the stimulation-ON and OFF conditions were shown in Figs. 6(B) and (C), respectively. As presented in Fig. 6(B), the $I_{F(560)}$ PA signals in the contralateral S1FL region at bregma + 1 mm decreased by 4.560 ± 0.005% from stimulation-OFF to stimulation-ON (Wilcoxon matched-pairs signed-rank test, $p=0.043$; $n=6$). Conversely,the $I_{F(560)}$ PA signals in the contralateral S1FL region at the bregma − 1.5 mm section and in the S1Tr region at the bregma − 2.5 mm section increased by about 2.230 ± 0.005% and 2.800 ± 0.001%, respectively, from simulation-OFF to stimulation-ON (Wilcoxon matched-pairs signed-rank test, $p=0.043$ and 0.042, respectively ; $n=6$). Similar results were also obtained for $I_{F(600)}$. The $I_{F(600)}$ PA signals in the contralateral S1FL region at bregma + 1 mm significantly decreased by 4.180 ± 0.007% from stimulation-OFF to stimulation-ON (Wilcoxon matched-pairs signed-rank test, $p=0.043$; $n=6$). During stimulation, PA signals in the contralateral S1FL region at bregma − 1.5 mm and in the contralateral S1Tr region at bregma − 2.5 mm significantly increased by 2.210 ± 0.004% and 2.370 ± 0.001%, respectively, (Wilcoxon matched-pairs signed-rank test, $p=0.043$ and 0.042, respectively; $n=6$), as shown in Fig. 6(C). There were no significant bilateral differences in $I_{F(560)}$ or $I_{F(600)}$ PA signals during stimulation-OFF (Wilcoxon matched-pairs signed-rank test, $p=0.821$; $n=6$). The bilateral differences in cortical contralateral S1FL at bregma + 1 and bregma − 1.5 mm and S1Tr at bregma − 2.5 mm were significant during stimulation-ON (Wilcoxon matched-pairs signed-rank test, $p=0.043$, 0.042 and 0.043, respectively; $n=6$).

Discussion

Characteristics of the current functional PAM system

In the visible spectral range, blood vessels have strong intrinsic optical absorption, i.e., strong PA signals. Therefore, to provide a high signal-to-noise ratio and to probe *in vivo* functional changes in blood vessels during electrical stimulation, the fPAM system used in this study adopted laser pulses at a visible spectral range instead of NIR for PA wave excitation. In the present study, optimal optical wavelengths (i.e., λ_{560}, λ_{570}, and λ_{600}) were used. When SO_2 levels change, the largest changes in blood absorption coefficients were observed at approximately λ_{560} and λ_{600} nm. That is, the detected PA signals at λ_{560} or λ_{600} were most sensitive to the SO_2 changes during stimulation. The wavelength λ_{570} was the isosbestic point of the molar extinction spectra of oxy- and deoxy-hemoglobin; hence, the detected PA signals at λ_{570} could serve as an oxygenation-insensitive reference. In addition, the 68 μm axial resolution obtained by the 25-MHz transducer in the fPAM system was smaller than the optical penetration depth (about 100 μm) in pure blood at the visible light region. Therefore, the PA signals detected by this transducer retained proportionality to the blood's optical absorption, which was the basis for quantitative probing of functional changes (Sivaramakrishnan et al., 2007). Details of optimal wavelength selection and the proportionality issue were provided in the Appendix.

Another important issue for functional brain imaging is system stability. The major source of system instability in the fPAM system is laser energy fluctuation. Since the signals are proportional to the laser energy coupled into the imaged objects, the stability of the PA signals is affected by laser energy fluctuation. In the present system, a photodiode was used to monitor the delivered laser energy and to compensate for PA signal variations caused by laser energy instability. With photodiode compensation, the root-mean-square stability of the detected PA signal was approximately 1.3% (Wang, 2009c). This was the detection limit of the current fPAM system for probing PA signal changes resulting from brain activation.

The image quality of the projected C-scan image in Fig. 3(B) was worse than those of images of mouse brains available in the literature (Stein et al., 2009). Such results could be attributed to the lateral resolution (~171 μm) of the commercially-available 25-MHz transducer in the fPAM system. In addition, the curvature of the cortex in the rat is larger than that of the mouse, causing difficulties in positioning the whole imaged cortex into the focal zone of the transducer. To offer better focus quality over the entire imaged area, scanning that follows the brain curvature (Zhang et al., 2007) or a synthetic aperture-focusing technique (Li et al., 2006) may be applied. Another problem demonstrated in Fig. 3(B) was that the quality of the large SSS vessel was not satisfactory. In Fig. 5(A), although the SSS can be seen in the PA B-scan images, the detected PA signals from the SSS were much weaker than those from other cortical vessels. Similar results were reported in Stein et al. (2008, 2009). Spherical geometric focusing and the finite detection bandwidth of the ultrasound transducer used may account for such results. The frequency of the PA signals generated by the SSS may be out of the detection bandwidth of the transducer. Sensing with spherical geometric focusing inherently preferred point-PA sources. However, it was not applicable to the SSS PA signals because of the large size of the SSS, thus weakening the detection of PA signals from the SSS.

The last concern was the limited scanning speed in the current fPAM system. In the current study, a single spherically-focused ultrasonic transducer with mechanical scanning and a 10-Hz pulse repetition-rate laser system was adopted. The use of a high-frequency ultrasound array system and a high pulse repetition-rate laser system could dramatically improve scanning speed, which may facilitate the imaging of transient responses during stimulation (Song et al., 2009). Moreover, although craniotomies were performed in this study, transcranial fPAM imaging for small animal models was also feasible (Stein et al., 2009; Wang, 2009a; Wang et al., 2003), with which would enable long-term tracking of functional changes caused by therapeutic interventions or drugs.

The advantages of the fPAM over established optical techniques are deeper penetration depth with high ultrasonic spatial resolution and intrinsic optical contrast, and are capable of accessing multiple physiological parameters regarding brain activation in a single setting. In addition to probing changes in SO_2 and CBV as demonstrated in this study, the fPAM can be also used to measure changes in blood flow speed (Yao et al., 2010), and vessel diameter (Kolkman et al., 2004) during stimulation. With SO_2, CBV, and blood flow speed, the fPAM can estimate the metabolic rate of oxygen (i.e., oxygen consumption rate) during stimulation with high spatial resolution and deep penetration. The feature of the deep penetration with high spatial resolution is also important for functional brain imaging since the responses of the functional imaging under the stimulation not only present in the superficial cortical layer but also may occur in the deeper area (Shih et al., 2009). Our future work will focus on transcranial functional brain imaging and imaging of deeper brain activation responses.

Investigation of the functional changes of $I_{R(570)}$ and $I_{F(560\ or\ 600)}$ by fPAM

According to the findings of optical absorption spectra, λ_{560} and λ_{600} are sensitive to SO_2 changes, whereas λ_{570} is insensitive to such changes. The $I_{R(570)}$ is sensitive to changes in CBV but insensitive to changes in SO_2, as shown in Fig. 5. The $I_{R(570)}$ contains other signals generated by different types of tissues, such as CBV. Therefore, to isolate SO_2 changes (e.g., excluding effects of CBV), PA images acquired at λ_{560} or λ_{600} were normalized to the data acquired at λ_{570}, which served as a reference for CBV changes. The $I_{F(560\ or\ 600)}$ only contains information related to changes in SO_2 levels, with the effects of CBV changes removed by normalization with $I_{R(570)}$ (as derived in the Appendix). Therefore, independent probes of changes in SO_2 and CBV could be achieved by the fPAM system, where $I_{R(570)}$ is used as a marker for CBV changes and $I_{F(560\ or\ 600)}$ as a marker for SO_2 changes.

Our findings during forepaw electrical stimulation showed significant increases in both SO_2 (i.e., negative $\Delta I_{F(560\ or\ 600)}$ or decreases in $I_{F(560\ or\ 600)}$) and CBV (i.e., increases in $I_{R(570)}$) in the S1FL region at bregma + 1 mm. The results corresponded well with previous DOI and fMRI studies (Culver et al., 2005; Devor et al., 2008; Grinvald et al., 1988; Keilholz et al., 2004, 2006; Liu et al., 2004; Shih et al., 2009; Siegel et al., 2003). In the present study, the novel functional PAM system directly measured SO_2 and CBV changes at 68×171 μm, a resolution that has yet been reliably or directly detected with other techniques. In addition, compared with the conventional BOLD fMRI technique that measures a mixed hemodynamic response, our data purely reflect activation-induced changes in SO_2. Results also revealed the fact that the strong BOLD responses detected in large draining veins may be mainly driven by alterations in SO_2 (Fig. 6). Furthermore, our findings supported results from previous fMRI and DOI studies, showing that SO_2 and CBV changes in the contralateral regions were significantly higher than in the ipsilateral side (Culver et al., 2005; Devor et al., 2008; Grinvald et al., 1988; Keilholz et al., 2004, 2006; Liu et al., 2004; Shih et al., 2009; Siegel et al., 2003).

Increases in $I_{F(560\ or\ 600)}$ (i.e., positive $\Delta I_{F(560\ or\ 600)}$) were found in the contralateral cortex at the bregma −1.5 mm and −2.5 mm sections during stimulation, indicating a decrease in SO_2 (Fig. 6). One explanation for such results was that blood mainly flowed into the activation area, leaving adjacent regions with lower SO_2 (Harel et al., 2002). However, it is intriguing that similar patterns were not observed among in CBV images (Fig. 5). Further investigations are warranted to better understand the brain hemodynamics during neuronal activation. The development of the current fPAM technique could also benefit from the interpretations of BOLD fMRI response. The BOLD signal is sensitive to the balance between oxygen delivery and consumption, both of which may occur during neuronal activation (Ogawa et al., 1990). It is also possible for a negative BOLD signal to occur under very high neuronal activity, when oxygen consumption far exceeds oxygen supply (Schridde et al., 2008). Therefore, the novel fPAM technique may be used to isolate the contribution of SO_2 from the BOLD signal, improving the accuracy of the interpretations of specific BOLD responses.

Another important issue was that significant changes in CBV and SO_2 signals were observed in S1Tr as well as S1FL regions. According to a previous study, BOLD signal changes could be evoked more easily from forepaws (with smaller currents) than from the tail or hindpaws (Spenger et al., 2000). The local cerebral blood flow response to forepaw stimulation is related to stimulation intensity, pulse width and stimulus frequency (Silva et al., 1999). In the present study, rats under a high current of stimulation may induce activations near the cortical brain regions, such as the S1Tr. Five major peripheral nerves pass through forepaws of rats, the musculocutaneous nerve, the lateral cutaneous nerve, the median nerve, the ulnar nerve, and the radial nerve (Cho et al., 2007). Cho et al. found that the cortical BOLD response to direct radial nerve stimulation (1.0 mA, 10 Hz, 1 ms) activated the S1Tr and the secondary somatosensory region (S2). In the present study, the high current stimulation applied to forepaws may have fired the radial nerve, resulting in the substantial activation in the S1Tr (Cho et al., 2007). In summary, the current fPAM system was successfully established for detecting brain PA signals in response to changes in neuronal activity induced by forepaw electrical

stimulation. The present study demonstrated that the fPAM system could provide novel SO_2 and CBV mapping in a single setting. *In vivo* measurements of brain hemodynamics with non-ionizing radiation, high intrinsic blood contrast of optical absorption, and good ultrasonic spatial resolution at deeper imaging depth are now available.

Acknowledgments

The authors are grateful to Po-Hsun Wang for his prior system development. We are greatly indebted to the National Science Council of Taiwan, R.O.C. for the support of this research through shares in grant nos. NSC 96-2220-E-009-029, NSC 97-2220-E-009-029, and NSC 97-2221-E-007-084-MY3. Furthermore, this work was supported in part by the Top University Program of MOE, Taiwan, R.O.C. and the Diamond Project of NCTU.

Appendix A

A.1. Multi-wavelength PA imaging to probe changes in blood volume and oxygenation

In rat blood, two forms of hemoglobin—oxy-hemoglobin and deoxy-hemoglobin (i.e., HbO_2 and Hb)—are the dominant absorption] in the visible spectral range. That is, in the visible spectral range, blood vessels have strong optical absorption, guaranteeing that the detected photoacoustic signals mainly come from vessels. For an optical wavelength λ, the photoacoustic signal detected by the ultrasound transducer can be written as

$$P_{\text{detected}}(\lambda,t) = P'(\lambda,t)\otimes h_e(t), \tag{A1}$$

where $h_e(t)$ is the electrical impulse response of the ultrasound transducer, and $P'(\lambda_i,t)$ is the PA wave reaching the transducer's surface. This wave is proportional to the optical absorption coefficient $\mu_a(\lambda)$ of blood:

$$p'(\lambda,t)\propto\mu_a(\lambda) = \varepsilon_{\text{Hb}}(\lambda)\cdot[\text{HB}] + \varepsilon_{\text{HbO}_2}(\lambda)\cdot[\text{HBO}_2], \tag{A2}$$

where $\varepsilon_{\text{Hb}}(\lambda)$ and $\varepsilon_{\text{HbO}_2}(\lambda)$are the molar extinction coefficients (in $\text{cm}^{-1}\,\text{M}^{-1}$) of Hb and HbO_2, respectively, and [Hb] and [HbO_2] are the concentrations of the two forms of hemoglobin.

From Eq. (A1), the factor affecting the proportionality of the detected signals to the optical absorption, as in Eq. (A2), is the electrical impulse response of the ultrasound transducer. It should be noted that to retain the proportionality of Eq. (A2), the electrical impulse response of the ultrasound transducer should be smaller than the optical penetration depth of blood at the selected excitation wavelength (e.g., ~100 μm at λ_{570}, assuming 45% hematocrit) (Sivaramakrishnan et al., 2007).

Fig. A showed the estimated absorption spectra of the blood specimen for differences of SO_2—95%, 90%, 85%, and 70%, where SO_2 is defined as $SO_2 = \frac{[HbO_2]}{[Hb]+[HbO_2]}$. In the visible spectral range, it was observed that the largest absorption changes occur approximately at λ_{560} and λ_{600} when the SO_2 level changes. At λ_{570}, the optical absorption insensitive to the SO_2 level, as shown in Fig. A, indicating an isosbestic point of the molar extinction spectra of oxy- and deoxy-hemoglobin. That is, the generated photoacoustic signals at λ_{560} and λ_{600} were sensitive to SO_2 changes, whereas those at λ_{570} were SO_2-insensitive. Since λ_{570} was an isosbestic point, PA signal changes at this wavelength dominantly resulted from changes in HbT (HbT = [HbO_2] + [Hb]), which are related to changes in blood volume (BV) and vessel diameter (VD) (Dunn et al., 2003; Sivaramakrishnan et al., 2007; Stein et al., 2009). Therefore, laser pulses at λ_{560}, λ_{570}, and λ_{600} were employed in this study. PA images at λ_{570} were used to probe the changes in CBV during electrical stimulation. To observe the effects of electrical stimulation on the SO_2 level (i.e., excluding effects of CBV), PA images acquired at λ_{560} or λ_{600} were normalized by that acquired at λ_{570}. The images served as a reference for CBV changes, assuming on a point-by-point basis that the detected PA signals $P_{\text{detected}}(\lambda,t)$ were proportional to $P'(\lambda,t)$:

$$\begin{aligned} I_{F(560\text{ or }600)} &= \frac{P_{\text{detected}}(560\text{ or }600\,\text{nm},t)}{P_{\text{detected}}(570\,\text{nm},t)} \\ &\propto \frac{\varepsilon_{\text{Hb}}(560\text{ or }600\text{nm})[\text{Hb}]+\varepsilon_{\text{HbO}_2}(560\text{ or }600\text{nm})[\text{HbO}_2]}{\varepsilon_{\text{Hb}}(570\,\text{nm})[\text{Hb}]+\varepsilon_{\text{HbO}_2}(570\,\text{nm})[\text{HbO}_2]} \\ &\cdot\frac{\varepsilon_{\text{Hb}}(560\text{ or }600\text{nm})(1-SO_2)+\varepsilon_{\text{HbO}_2}(560\text{ or }600\text{nm})SO_2}{\varepsilon_{\text{Hb}}(570\,\text{nm})} \end{aligned} \tag{A3}$$

where $\varepsilon_{\text{HbO}_2}(570\,\text{nm}) = \varepsilon_{\text{Hb}}(570\,\text{nm})$.

Fig. B showed $I_{F(560)}$ in Eq. (A3) as a function of SO_2 changes and indicated that $I_{F(560)}$ was inversely proportional to changes in SO_2. It

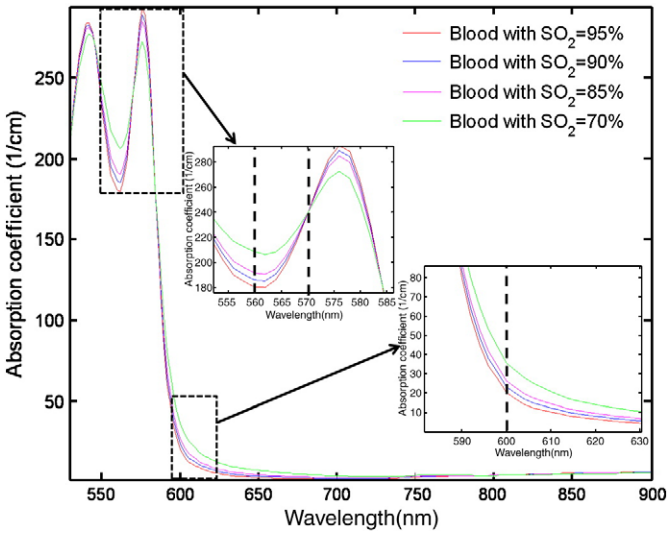

Fig. A. Estimated optical absorption spectra of blood with different levels of SO_2—95%, 90%, 85%, and 70%. Assuming the detected PA signals were proportional to the optical absorption coefficient of blood in the visible spectral range, the PA signals acquired at λ_{560} and λ_{600} were the most sensitive to SO_2 changes. On the other hand, those acquired at λ_{570} could serve as an oxygenation-insensitive reference in the current analysis, because λ_{570} was an isosbestic point of the molar extinction spectra of oxy- and deoxy-hemoglobin.

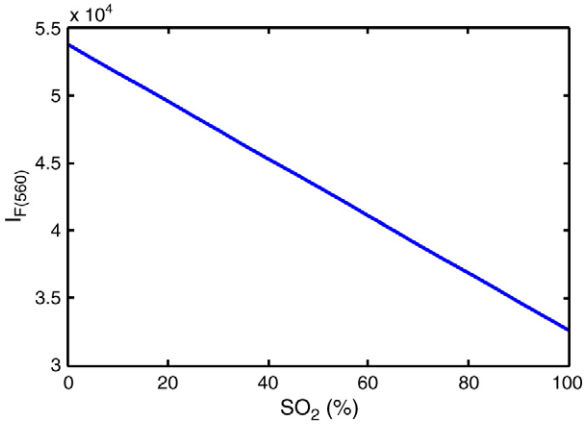

Fig. B. $I_{F(560)}$ was a function of SO_2 level, showing that $I_{F(560)}$ was inversely proportional to SO_2 during electrical stimulation. That is, $I_{F(560)}$ increases as SO_2 decreases. Note that this figure was calculated based on compiled molar extinction spectral data of oxy- and deoxy-hemoglobin provided by Oregon Medical Laser Center (http://omlc.ogi.edu) and an assumed typical hemoglobin concentration for whole blood—150 g Hb/liter.

could also be derived from Eq. (A3) by taking the differential of $I_{F(560)}$ over SO_2:

$$\Delta I_{F(560 \text{ or } 600)} \propto -\Delta SO_2, \quad \text{(A4)}$$

where Δ represents the differences and $\Delta I_{F(560 \text{ or } 600)}$is the difference of $I_{F(560)}$for different SO_2 levels. Eq. (A4) was also applicable for λ_{600}. That is, when SO_2 decreases, $I_{F(560 \text{ or } 600)}$ increases, as was observed by fPAM of the brain sections at bregma − 1.5 mm and bregma − 2.5 mm. The decrease in the SO_2 level during the stimulation indicated that the oxy- and deoxy-hemoglobin both increased, with the concentration increase of the deoxy-hemoglobin was larger than that of oxy-hemoglobin. It should be noted that Eq. (A4) was only applicable to excitation at λ_{560} or λ_{600} in this study. Rules for excitation at other wavelengths could be similarly derived.

References

Cho, Y.R., Pawela, C.P., Li, R., Kao, D., Schulte, M.L., Runquist, M.L., Yan, J.-G., Matloub, H.S., Jaradeh, S.S., Hudetz, A.G., Hyde, J.S., 2007. Refining the sensory and motor ratunculus of the rat upper extremity using fMRI and direct nerve stimulation. Magn. Reson. Med. 58, 901–909.

Cina, C., Katsamouris, A., Megerman, J., Brewster, D.C., Strayhorn, E.C., Robison, J.G., Abbott, W.M., 1984. Utility of transcutaneous oxygen tension measurements in peripheral arterial occlusive disease. J. Vasc. Surg. 1, 362–371.

Culver, J.P., Siegel, A.M., Franceschini, M.A., Mandeville, J.B., Boas, D.A., 2005. Evidence that cerebral blood volume can provide brain activation maps with better spatial resolution than deoxygenated hemoglobin. NeuroImage 27, 947–959.

Devor, A., Hillman, E.M.C., Tian, P., Waeber, C., Teng, I.C., Ruvinskaya, L., Shalinsky, M.H., Zhu, H., Haslinger, R.H., Narayanan, S.N., Ulbert, I., Dunn, A.K., Lo, E.H., Rosen, B.R., Dale, A.M., Kleinfeld, D., Boas, D.A., 2008. Stimulus-induced changes in blood flow and 2-deoxyglucose uptake dissociate in ipsilateral somatosensory cortex. J. Neurosci. 31, 14347–14357.

Dunn, A.K., Devor, A., Bolay, H., Andermann, M.L., Moskowitz, M.A., Dale, A.M., Boas, D.A., 2003. Simultaneous imaging of total cerebral hemoglobin concentration, oxygenation, and blood flow during functional activation. Opt. Lett. 28, 28–30.

Ermilov, S.A., Khamapirad, T., Conjusteau, A., Leonard, M.H., Lacewell, R., Mehta, K., Miller, T., Oraevsky, A.A., 2009. Laser optoacoustic imaging system for detection of breast cancer. J. Biomed. Opt. 14, 024007.

Fainchtein, R., Stoyanov, B.J., Murphy, J.C., Wilson, D.A., Hanley, D.F., 2000. Local determination of hemoglobin concentration and degree of oxygenation in tissue by pulsed photoacoustic spectroscopy. Proc. SPIE Int. Soc. Opt. Eng. 3916, 19–33.

Foo, S.S., Abbott, D.F., Lawrentschuk, N., Scott, A.M., 2004. Functional imaging of intratumoral hypoxia. Mol. Imaging Biol. 6, 291–305.

Gratton, G., Fabiani, M., 1998. Dynamic brain imaging: event-related optical signals (EROS) measures of the time course and localization of cognitive-related activity. Psychonomic Bull. Rev. 5, 535–563.

Grinvald, A., Frostig, R.D., Lieke, E., Hildesheim, R., 1988. Optical imaging of neuronal activity. Physiol. Rev. 68, 1285–1366.

Haacke, E.M., Lai, S., Reichenbach, J.R., Kuppusamy, K., Hoogenraad, F.G.C., Takeichi, H., Lin, W., 1998. In vivo measurement of blood oxygen saturation using magnetic resonance imaging: a direct validation of the blood oxygen level-dependent concept in functional brain imaging. Hum. Brain Mapp. 5, 341–346.

Harel, N., Lee, S.-P., Nagaoka, T., Kim, D.-S., Kim, S.-G., 2002. Origin of negative blood oxygenation level-dependent fMRI signals. J. Cereb. Blood Flow Metab. 22, 908–917.

Hyder, F., Behar, K.L., Martin, M.A., Blamire, A.M., Shulman, R.G., 1994. Dynamic magnetic resonance imaging of the rat brain during forepaw stimulation. J. Cereb. Blood Flow Metab. 14, 649–655.

Keilholz, S.D., Silva, A.C., Raman, M., Merkle, H., Koretsky, A.P., 2004. Functional MRI of the rodent somatosensory pathway using multislice echo planar. Magn. Reson. Med. 52, 89–99.

Keilholz, S.D., Silva, A.C., Raman, M., Merkle, H., Koretsky, A.P., 2006. BOLD and CBV-weighted functional magnetic resonance imaging of the rat somatosensory system. Magn. Reson. Med. 55, 316–324.

Kolkman, R.G.M., Klaessens, J.H.G.M., Hondebrink, E., Hopman, J.C.W., Mul, F.F.M.D., Steenbergen, W., Thijssen, J.M., Leeuwen, T.G.V., 2004. Photoacoustic determination of blood vessel diameter. Phys. Med. Biol. 49, 4745–4756.

Langham, M.C., Magland, J.F., Epstein, C.L., Floyd, T.F., Wehrli, F.W., 2009. Accuracy and precision of MR blood oximetry based on the long paramagnetic cylinder approximation of large vessels. Magn. Reson. Med. 62, 333–340.

Lee, M., Zaharchuk, G., Guzman, R., Achrol, A., Bell-Stephens, T., Steinberg, G.K., 2009. Quantitative hemodynamic studies in moyamoya disease. Neurosurg. Focus 26, 4.

Li, L., Zemp, R.J., Lungu, G., Stoica, G., Wang, L.V., 2007. Photoacoustic imaging of lacZ gene expression in vivo. J. Biomed. Opt. 12, 020504.

Li, M.-L., Zhang, H.F., Maslov, K., Stoica, G., Wang, L.V., 2006. Improved in vivo photoacoustic microscopy based on a virtual-detector concept. Opt. Lett. 31, 474–476.

Liu, Z.M., Schmidt, K.F., Sicard, K.M., Duong, T.Q., 2004. Imaging oxygen consumption in forepaw somatosensory stimulation in rats under isoflurane anesthesia. Magn. Reson. Med. 52, 277–285.

Mandeville, J.B., Marota, J.J.A., Kosofsky, B.E., Keltner, J.R., Weissleder, R., Rosen, B.R., Weisskoff, R.M., 2005. Dynamic functional imaging of relative cerebral blood volume during rat forepaw stimulation. Magn. Reson. Med. 39, 615–624.

Maslov, K., Stoica, G., Wang, L.V., 2005. In vivo dark-field reflection-mode photoacoustic microscopy. Optics Letter 30, 625–627.

Menon, C., Fraker, D.L., 2005. Tumor oxygenation status as a prognostic marker. Cancer Lett. 221, 225–235.

Nair, G., Duong, T.Q., 2004. Echo-planar BOLD fMRI of mice on a narrow-bore 9.4 T magnet. Magn. Reson. Med. 52, 430–434.

Ogawa, S., Lee, T.M., Kay, A.R., Tank, D.W., 1990. Brain magnetic resonance imaging with contrast dependent on blood oxygenation. P.N.A.S. 87, 9869–9872.

Oregon Medical Laser Center http://omlc.ogi.edu/.

Paxinos, G., Watson, Charles, 2007. The Rat Brain in Stereotaxic Coordinates. Academic Press, San Diego.

Schridde, U., Khubchandani, M., Motelow, J.E., Basavaraju, Sanganahalli, Hyder, F., 2008. Negative BOLD with large increases in neuronal activity. Cereb. Cortex 18, 1814–1827.

Shih, Y.-Y., Chen, Y.-Y., Chen, J.-C., Chang, C., Jaw, F.-S., 2007. ISPMER: integrated system for combined PET, MRI, and electrophysiological recording in somatosensory studies in rats. Nucl. Instrum. Methods Phys. Res., Sect. A 580, 938–943.

Shih, Y.-Y.I., Chang, C., Chen, J.-C., Jaw, F.-S., 2008. BOLD fMRI mapping of brain responses to nociceptive stimuli in rats under ketamine anesthesia. Med. Eng. Phys. 30, 953–958.

Shih, Y.-Y.I., Chen, C.-C.V., Shyu, B.-C., Lin, Z.-J., Chiang, Y.-C., Jaw, F.-S., Chen, Y.-Y., Chang, C., 2009. A new scenario for negative functional magnetic resonance imaging signals: endogenous neurotransmission. J. Neurosci. 29, 3036–3044.

Siegel, A.M., Culver, J.P., Mandeville, J.B., Boas, D.A., 2003. Temporal comparison of functional brain imaging with diffuse optical tomography and fMRI during rat forepaw stimulation. Phys. Med. Biol. 48, 1391–1403.

Silva, A.C., Lee, S.-P., Yang, G., Iadecola, C., Kim, S.-G., 1999. Simultaneous blood oxygenation level-dependent and cerebral blood flow functional magnetic resonance imaging during forepaw stimulation in the rat. J. Cereb. Blood Flow Metab. 19, 871–879.

Sivaramakrishnan, M., Maslov, K., Zhang, H.F., Stoica, G., Wang, L.V., 2007. Limitations of quantitative photoacoustic measurements of blood oxygenation in small vessels. Phys. Med. Biol. 52, 1349–1361.

Song, L., Kim, C.H., Maslov, K., Shung, K.K., Wang, L.V., 2009. High-speed dynamic 3D photoacoustic imaging of sentinel lymph node in a murine model using an ultrasound array. Med. Phys. 36, 3724–3729.

Spenger, C., Josephson, A., Klason, T., Hoehn, M., Schwindt, Ingvar, M., Olson, L., 2000. Functional MRI at 4.7 Tesla of the rat brain during electric stimulation of forepaw, hindpaw, or tail in single- and multislice experiments. Exp. Neurol. 166, 246–253.

Stein, E.W., Maslov, K., Wang, L.V., 2008. Noninvasive mapping of the electrically stimulated mouse brain using photoacoustic microscopy. P.N.A.S. 6856, 685654.

Stein, E.W., Maslov, K., Wang, L.V., 2009. Noninvasive, in vivo imaging of blood-oxygenation dynamics within the mouse brain using photoacoustic microscopy. J. Biomed. Opt. 14, 020502.

Tandara, A.A., Mustoe, T.A., 2004. Oxygen in wound healing—more than a nutrient. World J. Surg. 28, 294–300.

Wang, L.V., 2008. Tutorial on photoacoustic microscopy and computed tomography. IEEE J. Sel. Top. Quantum Electron. 14, 171–179.

Wang, L.V., 2009a. Multiscale photoacoustic microscopy and computed tomography. Nat. Photonics 3, 503–509.

Wang, L.V., 2009b. CRC. Photoacoustic Imaging and Spectroscopy.

Wang, L.V., Wu, H.-i., 2007. Biomedical Optics: Principles and Imaging. Wiley.

Wang, P.-H., 2009c. High Frequency Photoacoustic Imaging System and Its Applications in Small Animal Imaging. Department of Electrical Engineering. National Tsing Hua University.

Wang, X., Pang, Y., Ku, G., Xie, X., Stoica, G., Wang, L.V., 2003. Noninvasive laser-induced photoacoustic tomography for structural and functional in vivo imaging of the brain. Nat. Biotechnol. 21, 803–806.

Yao, J., Maslov, K.I., Wang, L.V., 2010. Transverse flow velocity measurement with photoacoustic Doppler bandwidth broadening. P.N.A.S. San Francisco, California, United States, p. 756402.

Zhang, H.F., Maslov, K., Stoica, G., Wang, L.V., 2006. Functional photoacoustic microscopy for high-resolution and noninvasive in vivo imaging. Nat. Biotechnol. 24, 848–851.

Zhang, H.F., Maslov, K., Wang, L.V., 2007. In vivo imaging of subcutaneous structures using functional photoacoustic microscopy. Nat. Protocols 2, 797–804.